A study of the Al-rich region of the Al–Fe–Ir alloy system

B. Grushko•

ERC-1, Forschungszentrum Jülich, 52425 Jülich, Germany

Abstract

Phase equilibria in Al–Fe–Ir were studied at 850 and 1100 °C above 50 at.% Al. The formation of the continuous ternary region of solid solutions was estimated along about 50 at.% Al between the Al–Fe and Al–Ir β-phases. The binary M-$Al_{13}Fe_4$ and Al_5Fe_2 phases dissolve up to at least 10 and 5 at.% Ir, the C_{Ir}-phase, Al_3Ir, χ_{Ir}-phase and Al_9Ir_2 up to ~4, ~9, ~2.5 and at least 2.5 at.% Fe, respectively. These binaries extend to the ternary compositions at approximately constant Al. Three ternary phases designated m, Ł and N were revealed. The m-$Al_{13}(Fe,Ir)_4$ phase of the $Al_{13}Os_4$-type structure (C2/*m*, a = 1.7406 nm, b = 0.41923 nm, c = 0.76459 nm, β = 115.78°) is formed at ~$Al_{75\text{-}76}Fe_{6\text{-}9}Ir_{18\text{-}15}$. A ternary hexagonal Ł-phase (a = 1.09034 nm, c = 0.77614 nm) is formed in a small compositional region around ~ $Al_{74}Fe_{14}Ir_{12}$. The structure of a complex ternary N-phase forming at ~$Al_{77.5}Fe_{5.0\text{-}10.5}Ir_{17.5\text{-}12}$ was not specified.

Keywords: Aluminum alloys; Transition metal alloys and compounds; Phase diagrams.

1. Introduction

No ternary Al–Fe–Ir phase diagram has been yet published. On the other hand, the boundary binary Al–Fe and Al–Ir alloy systems have been extensively studied.

The Al-rich region of the Al–Fe alloy system, relevant to the present report, has been again specified in two contributions published synchronously without mutual mentions [1a,b] and containing only some small differences in the configuration of the compositional regions of the phases.

• E-mail address: b.grushko@fz-juelich.de.

The recent results concerning the Al–Ir phase diagram and its individual phases have been included in Ref. [2] and used in the studies of the ternary alloy systems of Al–Ir with Co and Rh [3].

In the present work, the phase equilibria in Al–Fe–Ir are studied in the compositional region above 50 at.% Al at 850 and 1100 °C.

2. Experimental

Master alloys were produced by levitation induction melting in a water-cooled copper crucible under a pure Ar atmosphere. The purity of Al was 99.999 %, of Fe 99.99 %, of Ir 99.9 %. Additional alloys of intermediate compositions were similarly produced from the mixtures of the residuals of the samples studied previously.

The as-cast specimens were annealed at 1100 °C under an Ar atmosphere (99.999 % purity) or at 850 °C under vacuum (typically $9x10^{-7}$ mbar). The annealing times were up to 142 h at 1100 °C and up to 431 h at 850 °C. The as-cast and annealed samples were examined by powder X-ray diffraction (XRD) and scanning electron microscopy (SEM). The compositions of the phases were measured by energy-dispersive X-ray analysis (EDX) in SEM on polished unetched surfaces (JEOL 840a scanning microscope equipped with EDAX Genesis 200 emission spectroscopy system). Powder XRD examinations were carried out using Cu Kα1 radiation and an imaging plate (Huber G670). STOE software package was used for the indexing of the diffraction patterns and refinement of lattice parameters.

3. Results and discussion

3.1. Binary phases and their ternary extensions

The Al-rich region of the binary Al–Fe phase diagram in Fig. 1a is shown according to Ref. 1a. All Al–Fe phases exhibit visible binary compositional regions. A CsCl-type structure forming in the Al–Fe alloy system around the equiatomic composition (β-phase) is an extension of the disordered solid solution of Al in bcc Fe whose melting temperature continuously decreases with the increasing Al concentration. The Al-rich part of the Al–Fe phase diagram also contains the

equilibrium phases M-$Al_{13}Fe_4$, Al_5Fe_2, Al_2Fe, and the high-temperature Al_8Fe_5-phase. The crystallographic data of these phases are included in Table 1.

The Al-rich region of the Al–Ir phase diagram is shown in Fig. 1b according to Ref. [2], and around the equiatomic composition according to Ref. [4]. The congruent β-AlIr phase melting at 2120 °C only extends towards lower Al at elevated temperatures. In the Al-rich region of Al–Ir, there are the phases θ-Al_9Ir_2, φ-$Al_{45}Ir_{13}$, χ-$Al_{28}Ir_9$ (χ_{Ir}), Al_3Ir and C-$Al_{2.7}Ir$ (C_{Ir}) whose crystallographic data are included in Table 1.

Due to the existence of the isostructural Al–Fe and Al–Ir β-phases, the formation of the corresponding continuous ternary regions of solid solution is expected along about 50 at.% Al. The β-phase containing Fe:Ir ≈ 1:1 was observed experimentally.

A ternary region extended from the M-$Al_{13}Fe_4$ phase was observed up to ~10 at.% Ir, while the Al_5Fe_2 phase was found to dissolve up to ~5 at.% Ir (see Fig. 2). Neither of alloys containing possible ternary extensions of Al_2Fe and Al_8Fe_5 were studied. The ternary extensions of the C_{Ir}-phase, Al_3Ir, χ_{Ir}-phase and Al_9Ir_2 were revealed along almost constant Al up to ~4, ~9, ~2.5 and at least 2.5 at.% Fe, respectively.

3.2. Ternary phases and phase equilibria

Three ternary Al–Fe–Ir structures were revealed and designated in the following as N, m and *Ł*. The phase equilibria involving these ternaries and the above-mentioned binaries at 1100 °C and 850 °C are shown in Fig. 2a and Fig. 2b, respectively. The compositions of the phases forming in the studied alloys and the overall compositions of the alloys measured by SEM/EDX are marked in Fig. 2a,b by open squares and of by closed squares, respectively.

A single-phase sample was only obtained from the highest-Al N-phase ($Al_{77.5}Fe_{6.5}Ir_{16}$, see the powder XRD pattern in Fig. 3a), however the structures of the two other phases were easier encoded after the extraction of their powder XRD patterns from those in Fig. 3b and 3d, respectively.

The SEM/EDX examinations of a sample of $Al_{76.7}Fe_{7.3}Ir_{16}$ annealed at 1100 °C revealed a two-phase structure, where one of the phases exhibited the composition of the above-mentioned N-phase. By the subtraction of its powder XRD pattern (Fig. 3a) from that in Fig. 3b, the result indicated an $Al_{13}Os_4$–type monoclinic structure [5], which is also typical of the m-$Al_{13}Co_4$ phase

[3,6]. The reliability of this identification of the m-$Al_{13}(Fe,Ir)_4$ phase was confirmed by a simulation of its powder XRD pattern (see Fig. 3c) using the structural model of the m-$Al_{13}Os_4$ phase from Ref. [5]. The refined lattice parameters of the m-$Al_{13}(Fe,Ir)_4$ phase are included in Table 1.

The Al concentration of the m-$Al_{13}(Fe,Ir)_4$ phase, forming inside ~$Al_{75\text{-}76}Fe_{6\text{-}9}Ir_{18\text{-}15}$, is similar to that of the high-temperature m-$Al_{13}Co_4$ phase. The m-$Al_{13}Co_4$ phase was found to extend up to ~12 at.% Ir (see Fig. 2c), but at the ternary compositions, equivalent to those of the m-$Al_{13}(Fe,Ir)_4$ phase, the orthorhombic ε_{16}-type structure (ε in Fig. 2c) was revealed in Al–Co–Ir [3]. The M-$Al_{13}Fe_4$ phase, which coexists with m-$Al_{13}(Fe,Ir)_4$ at its ternary extension, is isostructural to monoclinic M-$Al_{13}Co_4$, which coexists with the m-$Al_{13}Co_4$ phase in binary Al–Co [3,6]. However, no solubility of Ir was revealed in the M-$Al_{13}Co_4$ phase, while the orthorhombic O-$Al_{13}Co_4$ phase was found to dissolve some Ir (see Fig. 2c).

The ternary Al–Fe–Ir *Ł*-phase was not associated with any of the binary or ternary Al-based structures revealed to date. It is formed in a small compositional region around ~$Al_{74}Fe_{14}Ir_{12}$. The powder XRD pattern of an $Al_{72.7}Fe_{12.8}Ir_{14.5}$ alloy containing the major *Ł*-phase is shown in Fig. 3d. According to SEM/EDX this alloy also contained some $Al_3(Ir,Fe)$, which could be easily recognized in the corresponding diffraction pattern, and the traces of β. Apart from the (*00l*) lines of $Al_3(Ir,Fe)$ (see Fig. 3e) no other overlaps of the lines of this minor phase were revealed. After the subtraction of the diffraction lines of $Al_3(Ir,Fe)$, the resulted pattern could be indexed for a hexagonal lattice (see Table 1 and Appendix)[1].

The structure of the above-mentioned N-phase was not specified. This phase was revealed in a compositional range of ~$Al_{77.5}Fe_{5.0\text{-}10.5}Ir_{17.5\text{-}12.0}$, close to the equivalent compositions of the Al–Co–Ir E-phase [3] and Al–Ru–Rh E-phase [7] (see Fig. 4, upper panel). On the other hand, its powder XRD pattern exhibited more similarities to that of a ternary N-phase revealed recently in Al–Fe–Pt [8] around ~$Al_{79}Fe_{12}Pt_9$ (see Fig. 4a,b vs. Fig. 4c). Subsequently it was also designated N. Attempts to index the powder XRD patterns of the both these N-phases using the structural model of the Al–Ru–Rh E-phase published in Ref. [9] were not successful. In contrast, the powder XRD patterns of the Al–Co–Ir E-phase (Fig. 4c) and Al–Co–Rh E-phase were reliably indexed in

[1] Alternatively, the powder XRD pattern could be indexed using a primitive orthorhombic lattice of a two times smaller volume: a = 0.94383(7) nm, b = 0.77596(4) nm, c = 0.54525(4) nm ($\Delta 2\theta$ = 0.008°, FOM(30) = 61.7).

Ref. [3] using the same structural model which is demonstrated by the comparison of the experimental and calculated diffraction patterns (see Fig. 4c,d). Similarly to that in the E-phases, the strong diffraction lines of the N-phases concentrate around the angular positions also typical of a decagonal phase with the periodicity of ~1.65 nm in the specific direction (D_4, see Fig. 4e [10]) pointing to the structural relation of these phases.

Another ternary orthorhombic phase, earlier revealed in Al–Fe–Pd [11], exhibited quite a similar powder XRD pattern (see Fig. 4f), where strong reflections are concentrated around the positions typical of the D_4-phase. This also-called N-phase is formed around a somewhat lower-Al composition (Fig. 4, upper panel). It was studied in Ref. [11] by powder XRD and electron diffraction The corresponding lattice parameters $a \approx 2.31$, $b \approx 1.60$ nm are close to those of the E-phases ($a \approx 2.35$ nm, $b \approx 1.65$ nm), but $c \approx 4.70$ nm is more than twice larger than $c \approx 2.00$ nm of the E-phases. In contrast to the E-phases, no structural model of the Al–Fe–Pd N-phase was deduced yet. The Al–Fe–Pt N-phase of Ref. [8] was designated just *expecting* structural relation to that in Al–Fe–Pd, where Pt would mainly replace Pd.

4. Summary

- Phase equilibria in Al–Fe–Ir were studied at 850 to 1100 °C above 50 at.% Al.
- The formation of the continuous ternary region of solid solutions was estimated along about 50 at.% Al between the Al–Fe and Al–Ir β-phases.
- M-$Al_{13}Fe_4$ and Al_5Fe_2 dissolve up to at least 10 and 5 at.% Ir, respectively.
- The C_{Ir}-phase, Al_3Ir, χ_{Ir}-phase and Al_9Ir_2 were found to extend along almost constant Al up to ~4, ~9, ~2.5 and at least 2.5 at.% Fe, respectively.
- The study revealed the formation of three ternary phases designated m, *Ł* and N.
- The ternary m-$Al_{13}(Fe,Ir)_4$ phase of the $Al_{13}Os_4$–type structure is formed at ~$Al_{75\text{-}76}Fe_{6\text{-}9}Ir_{18\text{-}15}$.
- A ternary hexagonal *Ł*-phase is formed in a small compositional region around ~ $Al_{74}Fe_{14}Ir_{12}$.
- The structure of a complex ternary N-phase forming at ~$Al_{77.5}Fe_{5.0\text{-}10.5}Ir_{17.5\text{-}12}$ was not specified.

Acknowledgement

The author thanks C. Thomas for technical contributions.

References

[1] a) Xiaolin Li, Anke Scherf, Martin Heilmaier, Frank Stein, J. Phase Equilibr. Diffus. 37 (2016) 162.

b) K. Han, I. Ohnuma, R. Kainuma, J. Alloys Comp. 668 (2016) 97.

[2] D. Pavlyuchkov, B. Grushko, T.Ya. Velikanova, Intermetallics. 16 (2008) 801.

[3] B. Grushko, J. Alloys Comp. 772 (2019) 399.

[4] C. Zhang, J. Zhu, Y. Yang, F. Zhang, Y.A. Ahang, Scripta Mater. 59 (2008) 403.

[5] L-E. Edshammar, Acta Chem. Scand. 18 (1964) 2294.

[6] X.L. Ma, U. Köster, B. Grushko, Z. Kristall. 213 (1998) 75.

[7] B. Grushko, D. Kapush, T.Ya. Velikanova, S. Samuha, L. Meshi, J. Alloys Comp. 509 (2011) 8018.

[8] B. Grushko, J. Alloys Comp. 829 (2020) 154444.

[9] S. Samuha, E. Mugnaioli, B. Grushko, U. Kolb, L. Meshi, Acta Crystal. B70 (2014) 999.

[10] D. Kapush, S. Samuha, L. Meshi, T.Ya. Velikanova, B. Grushko, J. Phase Equilibr. Diffus. 36 (2015) 327.

[11] S. Balanetskyy, B. Grushko, T.Ya. Velikanova, K. Urban, J. Alloys Comp. 376 (2004) 158.

Figure captions

Fig. 1. Binary phase diagrams of: a) Al−Fe according to Ref. [1a], b) Al−Ir according to Ref. [2,4].

Fig. 2. Partial isothermal sections of Al−Fe−Ir at 1100 °C (a) and 850 °C (b); and the overall compositions of the Al-rich Al−Co−Ir phases at 850-1100 °C (c) drawn from the data of Ref. [3]. L is the liquid. The regions of the phases N, m and *Ł* are marked by yellow, red and orange, respectively. Provisional lines are shown broken. The measured compositions of the phases are marked by open squares and of the alloys by closed squares. (In color in the web version).

Fig. 3. Powder XRD patterns (Cu Kα1 radiation): a) of $Al_{77.5}Fe_{6.5}Ir_{16}$ annealed at 850 °C, b) of $Al_{76.7}Fe_{7.3}Ir_{16}$ annealed at 1100 °C; c) calculated from the structural model of the $Al_{13}Os_4$ m-phase of Ref. [5] using the refined lattice parameters of the Al−Fe−Ir m-phase; d) of $Al_{72.7}Fe_{12.8}Pt_{14.5}$ annealed at 1100 °C, e) of Al_3Ir phase (the (*00l*) lines are marked, $l = 2n$). (In color in the web version).

Fig. 4. Upper panel: overall compositions of the Al−Fe−Ir N-phase and the E-phases and N-phases mentioned in the text. Lower panel: selected 2θ regions of the powder XRD patterns (Cu Kα1 radiation) of: a) the $Al_{77.5}Fe_{6.5}Ir_{16}$ N-phase (same as in Fig. 3a), b) the $Al_{79}Fe_{12}Pt_9$ N-phase of Ref. [6], c) the $Al_{77}Co_{11}Ir_{12}$ E-phase of Ref. [3], d) calculated from the structural model of Ref. [7] for the refined lattice parameters of the E-phase in (c), e) the $Al_{78}Ru_{16}Pt_6$ D_4-phase [10], f) the $Al_{76.6}Fe_{13.4}Pd_{10.0}$ N-phase of Ref. [11]. (In color in the web version).

Table 1. Binary and ternary phases in Al–Fe–Ir mentioned in the text and diagrams. TW – this work.

Phase	Space group	Lattice parameters			Ref. Comment
		a, nm *α,* °	*b,* nm *β,* °	*c,* nm *γ,* °	
θ-Al_9Ir_2	$P2_1/a$	0.63779 -	0.64318 94.78	0.87337 -	[2]
φ- $Al_{45}Ir_{13}$	*Pnma*	1.6771	1.2327	1.7437	[2]
χ-$Al_{28}Ir_9$	*P*31*c*	1.2286	-	2.7375	[2]
Al_3Ir	$P6_3/mmc$	0.4246 0.42185(2) 0.42216(6)	- - -	0.7756 0.77643(3) 0.77427(8)	[2] TW, $Al_{73.5}Fe_{6.0}Ir_{20.5}$ TW, $Al_{74}Fe_9Ir_{17}$
C-$Al_{2.7}Ir$	*P*23 *or* $Pm\bar{3}$	0.7674 0.76666(2)	- -	- -	[2] TW, $Al_{73.0}Fe_{4.5}Ir_{22.5}$
β	$Pm\bar{3}m$	0.28948 0.2985	- -	- -	[1a], $Al_{50}Fe_{50}$ [2], $Al_{50}Ir_{50}$
M-$Al_{13}Fe_4$	*C*2/*m*	1.5492 -	0.8078 107.69	1.2471 -	[1a]
		1.5509(3) -	0.8129(2) 107.77(2)	1.2522(3) -	TW, $Al_{75.5}Fe_{18.7}Ir_{5.8}$
		1.5497(3) -	0.8137(2) 107.64(2)	1.2495(3) -	TW, $Al_{76.0}Fe_{15.7}Ir_{8.3}$
Al_5Fe_2	*Cmcm*	0.76559	0.64154	0.42184	[1a]
Al_2Fe	$P\bar{1}$	0.48745 87.930	0.64545 74.396	0.87361 83.062	[1a]
Al_8Fe_5	$I\bar{4}3m$	0.89757	-	-	[1a], at 1120 °C
m-$Al_{13}(Fe,Ir)_4$	*C*2/*m* [a]	1.7406(2) -	0.41923(4) 115.78(7)	0.76459(6) -	TW, $Al_{76}Fe_8Ir_{16}$
N	?	?	?	?	TW, $Al_{77.5}Fe_{6.5}Ir_{16}$
Ł	$P6_3/m$ [b]	1.09034(9)	-	0.77614(5)	TW, $Al_{73.3}Fe_{13.5}Ir_{13.2}$

[a] S.G. is by analogy with the space group of the m-$Al_{13}Os_4$-phase [5].
[b] S.G. is provisional.

Appendix. Diffraction data of the *Ł*-phase. S.G. = $P6_3/m$ (provisional). Refined lattice parameters: a = 1.09034(9) nm, c = 0.77614(5) nm. Aver. Δ2θ = 0.009°, Max. Δ2θ = 0.047°, FOM(30) = 81.8 from the total 54 lines. The sample contained minor Al_3Ir and traces of the β-phase, whose lines were excluded. The intensities marked by (*) are estimated due to the overlap with the reflections of Al_3Ir. The reflections with I/I_0<5% are not included.

No.	*h*	*k*	*l*	I/I_0	d, nm
1	2	0	0	22	0.47194
2	1	1	1	24	0.44608
3	0	0	2	12*	0.38803
4	2	1	0	28	0.35694
5	2	1	1	100	0.32431
6	2	0	2	9	0.29982
7	2	1	2	7	0.26260
8	3	1	0	5	0.26181
9	3	1	1	8	0.24812
10	3	1	2	48	0.21712
11	2	1	3	87	0.20949
12	4	1	0	31	0.20606
13	4	0	2	13	0.20168
14	3	0	3	10	0.19980
15	4	1	1	31	0.19916
16	0	0	4	7*	0.19405
17	3	2	2	18	0.18916
18	4	1	2	25	0.18203
19	4	2	1	8	0.17392
20	3	2	3	7	0.16609
21	4	2	2	5	0.16212
22	4	1	3	8	0.16118
23	3	1	4	5	0.15591
24	6	0	1	5	0.15422
25	4	2	3	9	0.14688
26	4	3	2	7	0.14409
	6	1	0		
27	4	1	4	19	0.14125
28	6	1	2	8	0.13497
	7	0	0		
	2	2	5		
29	4	4	1	5	0.13422
30	7	0	1	9	0.13289
31	7	0	2	6	0.12740
32	6	2	2	12	0.12403
	4	1	5		
33	3	0	6	8	0.11960
	7	0	3		

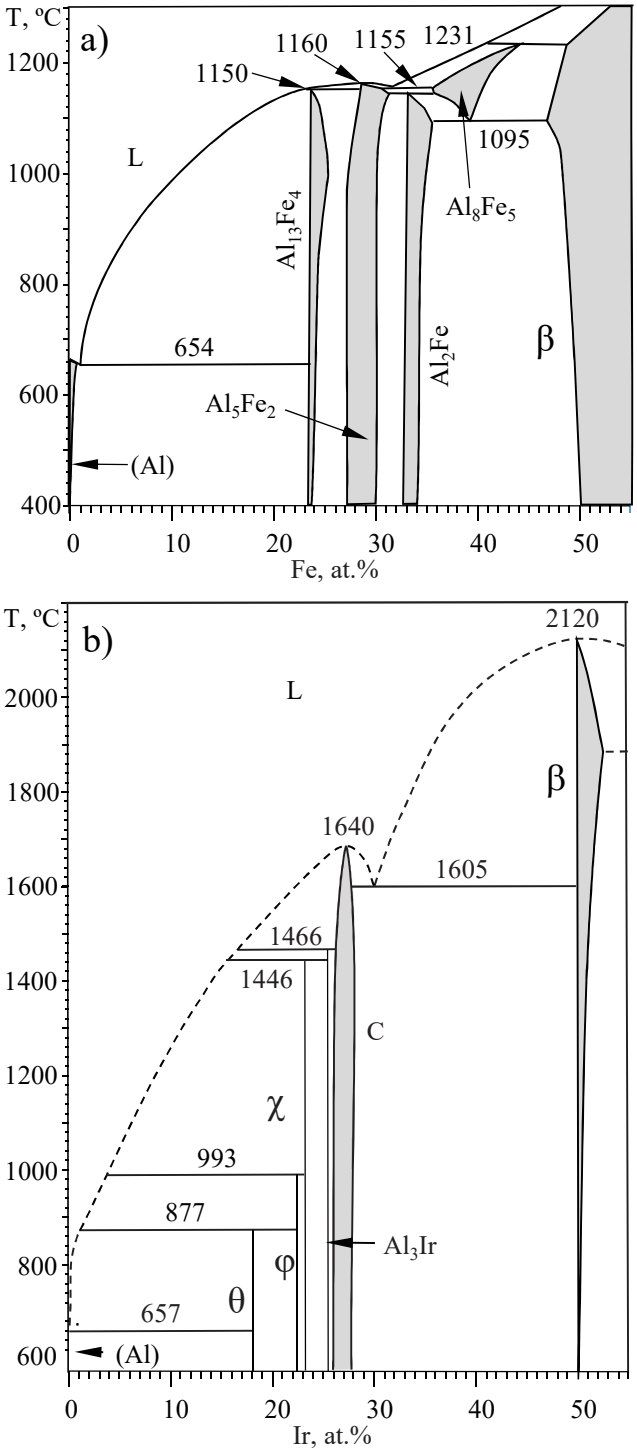
a)
T, ºC
1200
1000
800
600
400
1160
1155
1231
1150
1095
L
$Al_{13}Fe_4$
Al_8Fe_5
Al_2Fe
β
654
Al_5Fe_2
(Al)
0
10
20
30
40
50
Fe, at.%
b)
T, ºC
2000
1800
1600
1400
1200
1000
800
600
2120
L
β
1640
1605
1466
1446
C
χ
993
877
φ
θ
657
Al_3Ir
(Al)
0
10
20
30
40
50
Ir, at.%

Fig. 1

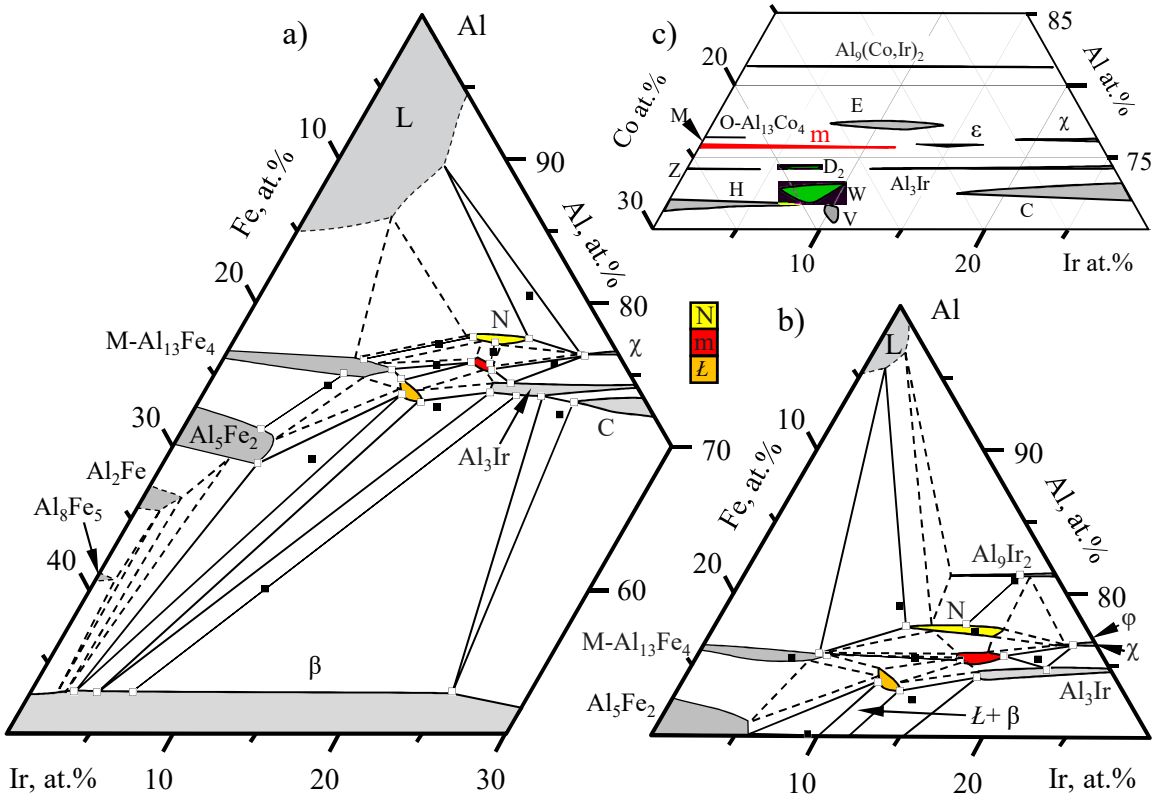
a)
Al
L
Fe, at.%
Al, at.%
M-Al13Fe4
Al5Fe2
Al2Fe
Al8Fe5
N
χ
C
Al3Ir
β
Ir, at.%
c)
Al9(Co,Ir)2
Co at.%
Al at.%
Ir at.%
M
O-Al13Co4
m
E
ε
χ
Z
D2
H
W
V
Al3Ir
C
N
m
Ł
b)
Al
L
Fe, at.%
Al, at.%
Al9Ir2
N
φ
χ
M-Al13Fe4
Al5Fe2
Al3Ir
Ł+ β
Ir, at.%

Fig. 2

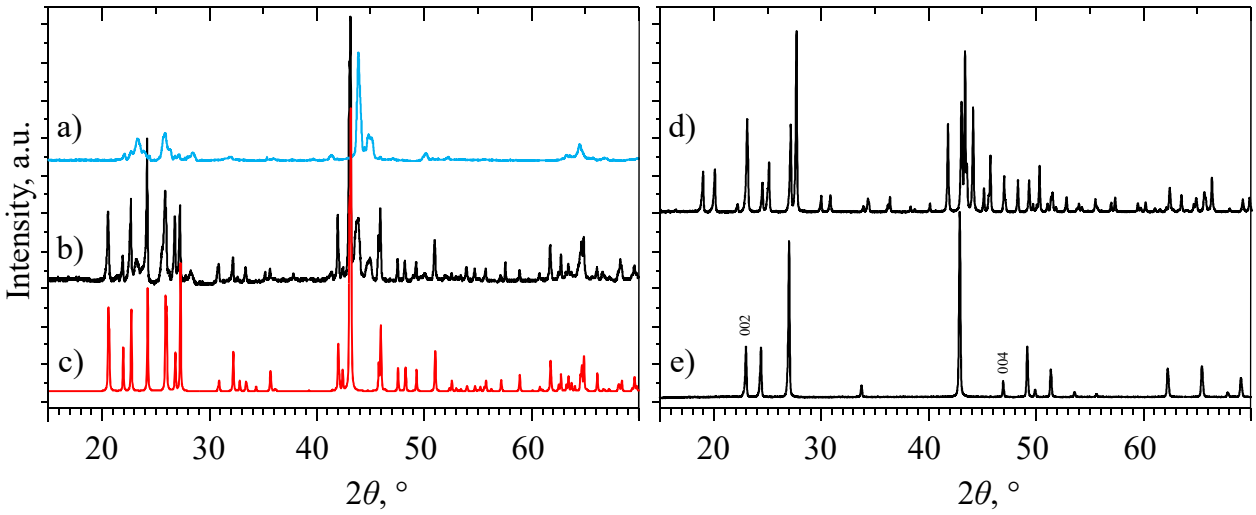

Fig. 3

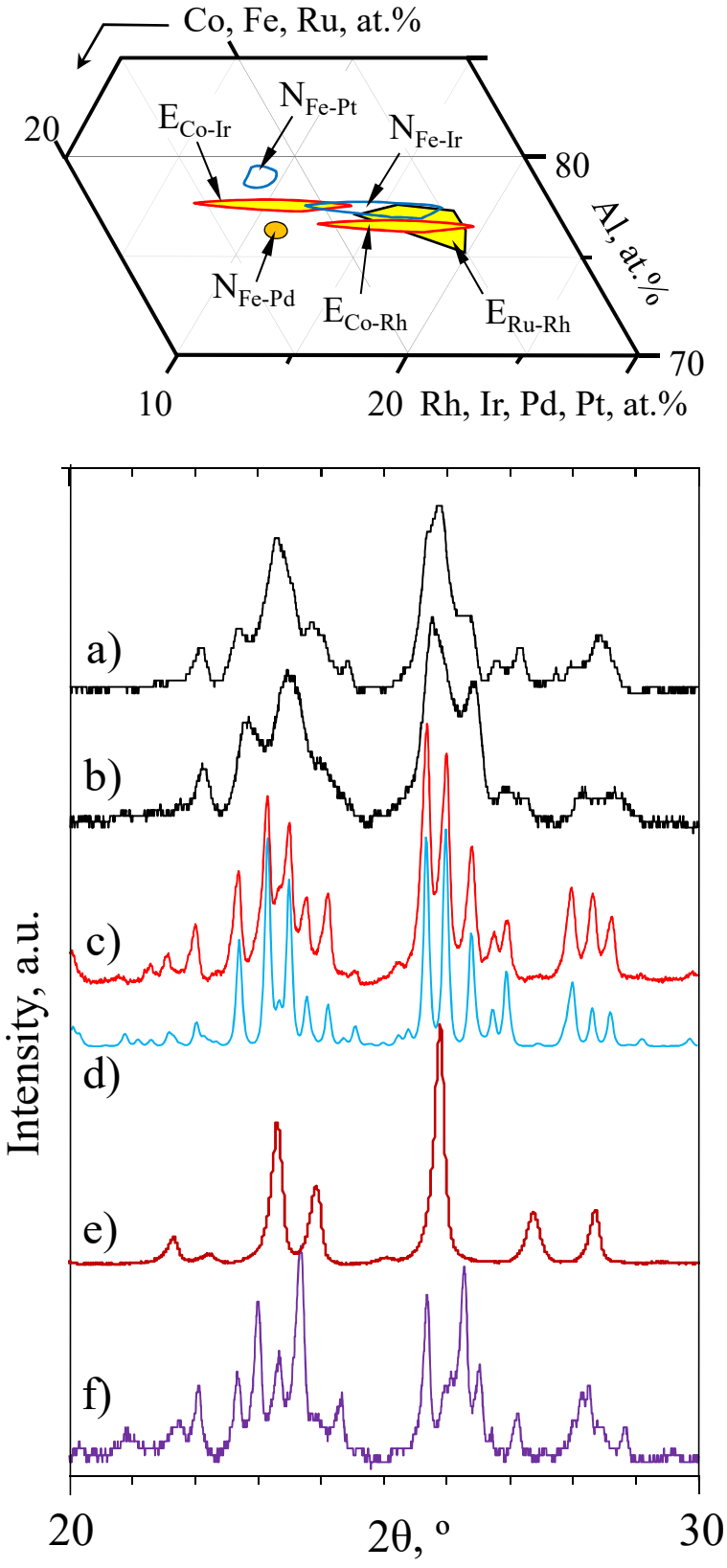
Co, Fe, Ru, at.%
20
80
Al, at.%
70
10
20 Rh, Ir, Pd, Pt, at.%
E_{Co-Ir}
N_{Fe-Pt}
N_{Fe-Ir}
N_{Fe-Pd}
E_{Co-Rh}
E_{Ru-Rh}
a)
b)
c)
d)
e)
f)
Intensity, a.u.
20
2θ, °
30

Fig. 4